Determination of two-dimensional temperature and additive density distributions in a high-intensity-discharge lamp arc

G. L. Rogoff, A. E. Feuersanger, J. P. Drummey, and H. L. Rothwell Jr.

Citation: Journal of Applied Physics **62**, 4084 (1987); doi: 10.1063/1.339121
View online: http://dx.doi.org/10.1063/1.339121
View Table of Contents: http://scitation.aip.org/content/aip/journal/jap/62/10?ver=pdfcov
Published by the AIP Publishing

Determination of two-dimensional temperature and additive density distributions in a high-intensity-discharge lamp arc

G. L. Rogoff, A. E. Feuersanger, and J. P. Drummey
GTE Laboratories Inc., Waltham, Massachusetts 02254

H. L. Rothwell, Jr.
GTE Electrical Products, Salem, Massachusetts 01970

(Received 12 May 1987; accepted for publication 13 July 1987)

Demixing of additive species can lead to significant axial and radial nonuniformities in the electrical and radiative characteristics of a vertical high-pressure arc. An optical emission method has been developed to determine both the radial and axial distributions of temperature and additive density as well as the pressure in a rotationally symmetric, enclosed arc in local thermodynamic equilibrium. The method can be used if one knows the vaporized quantity of the major component of the gas mixture in the arc tube. The procedure has been demonstrated by applying it to an ac 175-W Na-Sc-Hg lamp arc, with mercury the major component and sodium the additive of interest. An optically thin Hg line and an optically thin portion of the broadened Na *D* line were used. The resulting distributions clearly show the effects of segregation; the upper portion of the arc and the axial regions are significantly depleted of sodium.

I. INTRODUCTION

Segregation of additive species can lead to significant nonuniformities in the internal electrical and radiative properties of a high-pressure arc. For example, in vertically operating metal halide lamp arcs, which contain relatively small amounts of metal additives in high-pressure mercury, the metal additives are not distributed uniformly along the axis of the arc. For ac arcs this results primarily from the interaction of (a) natural convection due to large temperature gradients, (b) radial partial pressure gradients due to chemical reactions, and (c) radial cataphoresis due to space-charge electric fields associated with ambipolar diffusion; convection sweeps the additives upward with the hot gas in the core and downward with the cooler gas near the walls, while the radial forces drive the additives from the upwardly flowing central region to the downwardly flowing peripheral region before they reach the upper portion of the arc tube. As a result, the additives are concentrated in the lower portion of the arc. (Axial cataphoresis can be an important contributor to axial segregation in dc operation and can modulate the gross segregation in ac arcs.)

In order to improve the operating characteristics and efficiency of metal-halide arc lamps, which are commercially important light sources, considerable effort has been made to determine the distributions[1,2] of additives in metal halide arcs and to understand the processes[3–5] controlling those distributions. This paper describes an optical method for determining radial and axial temperature and density distributions in such arcs. The method can also be used for other types of arcs in gas mixtures containing a dominant component, e.g., a mixture dominated by a rare gas or atomic mercury.

Previously used techniques for measuring metal-halide arc temperatures and additive densities include laser scattering,[6,7] laser absorption,[8] and emission spectroscopy in optically thick spectral regions.[6,9] However, most efforts have used optically thin emission,[6,10–12] since the collection and interpretation of such emission data are usually considerably simpler than for the alternatives. To our knowledge, no previous emission studies of enclosed, wall-stabilized arcs have included axial variations in the analysis procedure.

An experimental method has been developed to determine self-consistent radial and axial distributions of temperature and additive density in a rotationally symmetric arc in local thermodynamic equilibrium (LTE). The pressure is determined along with the distributions. The method makes use of measured radiation emission coefficients coupled to a volume integration to account for the known quantity of the dominant component of the vapor. The procedure has been demonstrated by applying it to a vertical 175-W Na-Sc-Hg lamp arc, mercury being the major component in the mixture and sodium being the additive of interest. The arc, which is similar to that in a standard 175-W Sylvania Metalarc® lamp, is operated at 60 Hz. When the arc reaches steady state, the predetermined mercury dose is totally vaporized, while a condensed reservoir remains for the sodium. Thus, the total number of free mercury atoms in the arc tube is known. For the demonstration we used the optically thin Hg line at 577 nm and an optically thin portion of the broadened Na *D* line. Use of the latter avoids the common problem of isolating an interference-free Na line.

Section II outlines the general procedure for obtaining a set of radial temperature and density profiles at an arbitrary number of axial locations in an arc. Section III describes the application of the method to a metal-halide lamp arc, while Sec. IV presents and discusses the results of this application. The Appendix outlines the derivation of the sodium emission coefficient.

 0021-8979/87/224084-06$02.40

II. GENERAL PROCEDURE

The procedure consists essentially of the following steps:

(1) Transverse emission intensity scans are obtained for the major (buffer) species and additive species of interest at several axial locations.

(2) The measured absolute intensities are converted to radial distributions of emission coefficients. If the emission scans are made in optically thin spectral regions, an Abel inversion can be used to generate the emission coefficients from the intensity scans.

(3) The emission coefficients of the buffer are used to determine the pressure (which is taken to be uniform) and the radial temperature distributions at the selected axial locations. The iteration outlined in Fig. 1 is used here. In that iteration the value of pressure is adjusted until the pressure value and the corresponding temperature distributions yield, by volume integration, the known number of buffer atoms.

(4) The resulting temperature profiles are utilized along with the additive emission coefficients to determine the additive density profiles at those same axial locations.

Some of the steps in the procedure for determining the two-dimensional temperature distribution are similar to those used previously[13] for axially uniform temperature distributions.

In the demonstration of the procedure described here, the intensities were obtained from densitometer scans of spectrally-filtered arc photographs, and time-averaged distributions were generated.

III. SODIUM-MERCURY DEMONSTRATION

The method has been applied to a vertical 175-W Na-Sc-Hg arc operating at 60 Hz. The arc was regulated by an electronic ballast with a square-wave current output. In steady-state operation the predetermined mercury dose is totally vaporized, fixing the total number of mercury atoms in the vapor, while a condensate of the additives remains. The arc was contained in a quartz envelope of dimensions indicated in Fig. 2. The arc tube was dosed with 28 mg of mercury, an excess of sodium iodide and scandium iodide, and 45 Torr of argon for starting. The arc operated at a current of about 1.4-A rms and a voltage of about 119-V rms.

Side-on time-integrated photographic arc images were recorded, one made with mercury emission through a narrow-band filter at 577 nm to determine the temperature distribution, and one with sodium emission through a filter at 593 nm in the far red wing of the D line to determine the Na

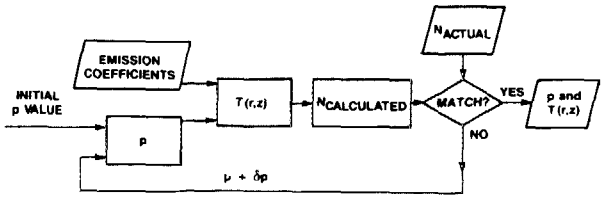

FIG. 1. Flow diagram for the iteration procedure to match the calculated buffer fill to the known fill. A volume integration is used to evaluate N_{calc}.

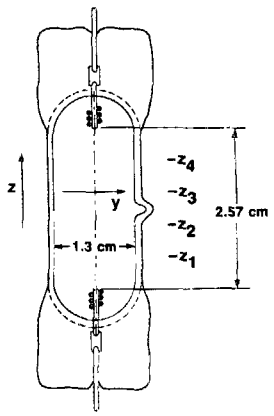

FIG. 2. Arc tube dimensions and locations of transverse scans. The distance between adjacent scans and between the end scans and the electrode tips is 0.51 cm.

density distribution. Both spectral regions are reasonably optically thin.[14] The photographs were made with an exposure time of $\frac{1}{30}$ s. Thus, images are integrated over two cycles.

The arc tube was imaged to fill the frame of a 35-mm camera containing Kodak Technical Pan 2415 film, a black and white film on a dimensionally stable Estar base which can be developed over a wide range of speeds and contrasts. The selected development resulted in a wide exposure range of the film (a relative exposure of 1000:1) to accommodate the wide brightness range encountered in the arc scans. Neutral density filters were used with both narrow-band filters to attenuate the radiation to a range appropriate for operation mostly in the midtone portion of the film response curve (film density versus absorbed energy density). To facilitate calibration of the film density, the film was exposed periodically to a photographic density step wedge (calibrated by Kodak). The optical arrangement and conditions, i.e., distances and apertures, were held fixed throughout the calibration and the measurements. The angular spread of rays was kept small to ensure proper filter operation and reliability of the Abel inversion.

Figures 3 and 4 show the spectral regions of interest for mercury and sodium, respectively, along with the transmission curves for the narrow-band filters. For the Hg 577-nm line we relate the power transmitted by the filter to the total emission from the line, i.e., with a Lorentzian line shape assumed as indicated by the dashed curve in Fig. 3. The ratio

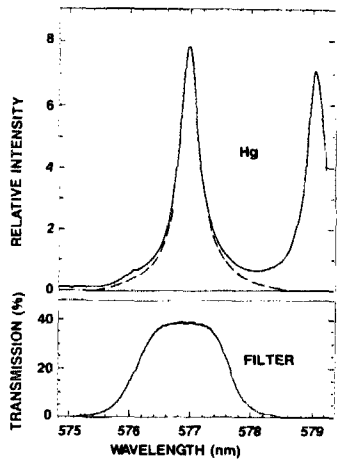

FIG. 3. Spectral distributions of the mercury 577.0-nm line and the filter transmission. To determine the total energy in the emission line from the energy transmitted we assumed a Lorentzian line shape, as indicated by the dashed line in the mercury spectrum. The resolution for the emission spectrum is 0.025 nm; the resolution for the filter scan is 0.05 nm.

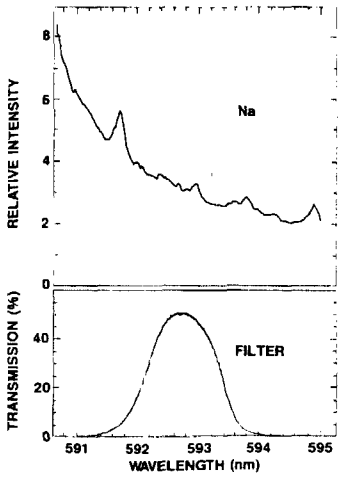

FIG. 4. Spectral distribution of the portion of the red wing of the sodium D line of interest and the corresponding filter transmission. The resolutions are the same as for Fig. 3.

of the total area under the 577-nm line to the area under the transmitted spectrum was taken to be independent of position in the transverse scan. (The ratio was determined experimentally at several transverse locations to support this.) The filter temperatures were monitored to ensure fixed transmission characteristics.

To calibrate the system for absolute intensity measurements, we used a tungsten strip radiator operated with a well-regulated dc current. The temperature in a selected region of the ribbon was measured using a disappearing-filament micro-optical pyrometer, with emissivity corrections applied to relate the pyrometer measurements at 0.65 μm to the emission at the Hg and Na wavelengths of interest. To establish the relationship between the film density and the radiant energy transmitted by each filter during the exposure, the tungsten reference source was photographed separately through the two narrow-band filters with a wide range of exposure times.

A calibrated microdensitometer was used to scan the photographic negatives at four axial locations on each arc image, as indicated in Fig. 2, with the output voltage digitized for computer data processing. The transverse mercury intensity distributions are strongly peaked at the center and decrease to background levels about halfway to the wall; as described below, a modified parabola is used to extend the temperature distributions to the wall. The sodium intensity distributions are relatively flat and extend closer to the walls.

The digitized microdensitometer output consists of 1100 values spaced uniformly across 13 mm, the tube diameter. In preparation for the Abel inversion, this output is first smoothed by averaging each point with the ten points preceding it and the ten points following it. A base level is then specified by a straight line between the background levels at the ends of the scan. After a central axis is determined—by the maximum in the mercury scan and by the midpoint of the sodium intensity distribution—half of each intensity profile is used (the same half for all scans) to avoid including image artifacts due to arc tube reflections. For each resulting half profile, a cutoff radius is specified by identifying the position where the intensity level has decreased to a given fraction of the maximum value (nominally 0.01). The resulting profile is described by 21 equally spaced points for convenient use of the Abel inversion routine described by Barr[15] to generate emission coefficients as a function of radius.

As indicated in Sec. II, the subsequent analysis procedure consists of two parts: (a) the mercury emission coefficients are used to determine the two-dimensional temperature distribution and the pressure and (b) the sodium emission coefficients and the temperature distribution are used to determine the sodium density distribution. Thus, the treatment of the Hg and the Na data is similar through the Abel inversion calculation. Thereafter, however, the steps differ.

The mercury emission coefficient is a function of the local temperature and the local mercury density. Since mercury dominates the vapor, we assume that the total pressure is given by the mercury pressure, and we express the mercury emission coefficient as a function of temperature and pressure, the latter being independent of position. Using an initial estimate of pressure (see Fig. 1), we calculate a corresponding set of radial temperature distributions from the emission coefficients and use those temperatures with the perfect gas law to obtain density distributions. We then integrate the densities over the tube volume to obtain a total number of mercury atoms, N. After comparing N with the known mercury fill, we change the value of pressure and repeat the process. With pressure steps of 100 Torr, this iteration continues until we obtain the calculated N closest to the known value. The result is a value for the total pressure and a set of temperature profiles for different axial locations. (For the results presented, the agreement in N is within 1%, which corresponds to an uncertainty in pressure of about 50 Torr.) The sodium emission coefficient is a function of the local temperature and the local sodium density. To determine the latter from the emission coefficients, we use the temperature distributions obtained from the iteration procedure.

The required expression for the frequency-integrated emission coefficient (power radiated per unit volume per unit solid angle) for the 577.0-nm mercury line is obtained from the relationship

$$\epsilon_{\mathrm{Hg},\Delta\nu}(r,z) = (4\pi)^{-1} n^*(r,z) h\nu_0 A, \tag{1}$$

where n^* is the number density of Hg atoms excited to the 6^3D_1 level, $h\nu_0$ is the energy of the atomic transition, and A is the transition probability. Assuming a Boltzmann distribution for the excited states, we can write for the density n^*

$$n^*/n_{\mathrm{Hg}} = (g^*/\overline{U})\exp(-V^*/kT), \tag{2}$$

where n_{Hg} is the total number density of Hg atoms, g^* is the statistical weight of the upper (6^3D_1) level, V^* is the energy of that level, and $\overline{U}$ is a representative value of the partition function.[16] Combining Eqs. (1) and (2) and expressing n_{Hg} in terms of the mercury pressure p_{Hg}, we obtain for the frequency-integrated emission coefficient

$$\epsilon_{\mathrm{Hg},\Delta\nu}(r,z) = (4\pi)^{-1} h\nu_0 A \frac{g^*}{\overline{U}} \frac{p_{\mathrm{Hg}}}{kT(r,z)} e^{-V^*/kT(r,z)}. \tag{3}$$

The emission coefficient is determined out to a maximum radius R_m determined by the densitometer sensitivity and the background intensity due to scattered light. Beyond

that radius, the temperature distribution is described by the modified parabola

$$T(r) = T_w + (T_\beta - T_w)\left[1 - (r/R_w)^\alpha\right],$$
$$R_m \leqslant r \leqslant R_w, \tag{4}$$

where R_w is the tube radius and T_w is the wall temperature. The two adjustable parameters T_β and α allow both the value and slope of the temperature distribution at the cutoff radius R_m to be matched. The slope at radius R_m is determined from the outermost two temperature values obtained from the mercury emission coefficients. The wall temperature[17] was taken to be 1000 K.

A volume integral is evaluated numerically to calculate the total number of mercury atoms in the arc tube. For this integration we describe the tube as a uniform cylinder with smaller cylindrical end regions containing the electrodes, with the volume of the simplified shape equaling that of the actual envelope. The temperature distribution at each scan location is assumed to extend axially halfway to the adjacent scan locations, or, for the outermost scan locations, to the beginning of the end regions. While the calculated temperature profiles are used for the main body of the envelope, a linear radial variation is used for the end regions, with a wall temperature of 950 K and an axial temperature of 1500 K to approximate an average electrode temperature. The electrode temperature[18] actually ranges from about 2300 K at the tip to about 850 K at the inside surface of the quartz.

The derivation of the sodium emission coefficient is similar to the mercury derivation, but because a continuum band is used, several additional relationships are needed. An outline of the derivation is included in the Appendix.

IV. RESULTS AND DISCUSSION

Figures 5(a) and 5(b) show, respectively, the resulting temperature and sodium density distributions. The small circles along the z axis indicate the locations of the electrode ends, the near circle representing the lower electrode, and the arrows in both plots of Fig. 5 indicate the cutoff radii for the temperatures obtained from the mercury emission coefficients; that is, the modified parabola is used for the temperature beyond those radii. The cutoff radii for the sodium densities are not shown since they lie beyond the region of plotted densities. The densities simply increase monotonically to the sodium cutoff radii. (Somewhere beyond those cutoff radii the Na density decreases rapidly with increasing radius.) Thus, the density plots have been truncated to display the more interesting density variations in the central region more clearly. Note that those density variations lie within the mercury cutoff radii, i.e., in the region of available mercury data rather than the region of the parabolic temperature extension. The mercury pressure obtained from the analysis is 4300 Torr.

The effect of segregation is evident in Figs. 5 and 6, the latter showing the axial variations of temperature and sodium number density. The sodium depletion on the axis increases with increasing z, and the radial extent of the depletion region expands with increasing z. The dearth of the easily ionized species in the upper portion of the arc leads to higher required operating temperatures in that region. The

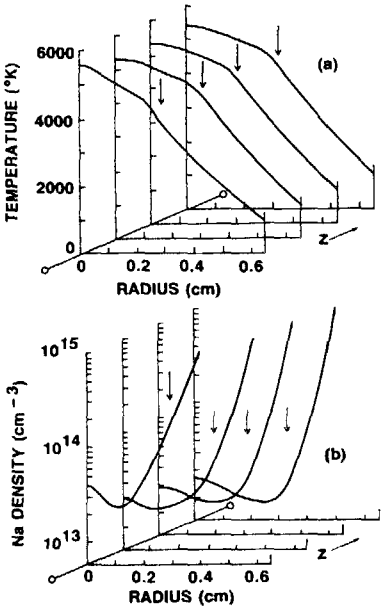

FIG. 5. (a) Temperature profiles at the selected axial locations. (b) Neutral sodium density profiles at the selected axial locations. In both plots the small circles along the z axis indicate the locations of the electrode tips, the circle in the foreground representing the lower electrode. The smooth curves were drawn through data points separated by about 0.03 cm. The arrows are explained in the text.

increase in the axial temperature near the bottom of the arc presumably reflects the constriction of the arc as it approaches the lower electrode tip. The temperature profiles indicate a slight "shouldering." Previous investigators[19] have attributed similar structure to metal additive recombination.

All four sodium density profiles exhibit a local maximum at the axis. That maximum might be due to convection and segregation. In the natural convective circulation, the hot mercury near the axis rises while the cooler vapor near the walls moves downward. After the sodium is swept along with the mercury downward along the side walls to the bottom of the tube, it is carried back upward into the arc in the axial region near the lower electrode. Thus, a local increase in the sodium density in that region is not surprising. As the sodium moves upward along the axis, radial partial pressure gradients and ambipolar diffusion act to transport sodium from the upwardly flowing vapor near the axis to the downward flow near the walls. Thus, the decrease in sodium density on the axis and the radially outward shift of the minimum in that density with increasing z is consistent with the convection/segregation picture.[20]

The density plotted in Fig. 5(b) is the density of sodium neutrals. At the temperatures reached near the axis of the arc, however, most of the available sodium atoms are ion-

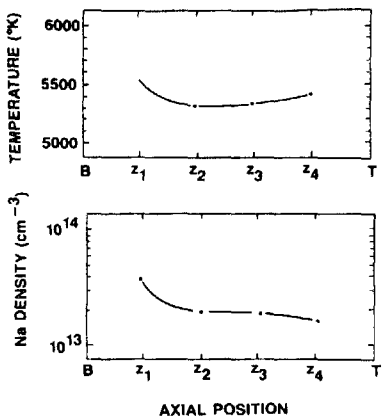

FIG. 6. Variations of temperature and sodium density along the tube axis. B and T denote bottom and top, respectively.

ized,[2] and the fraction ionized is a strong function of temperature. The total sodium density (neutrals plus ions) was calculated by applying the Saha equation[21] to the sodium neutral densities over the spatial regions covered in Fig. 5(b). The results indicated that as the neutral density decreases radially from its maximum on the axis, so does the total sodium density, while in the outer, cooler regions of the arc a relatively small fraction of the sodium is ionized and the total density is represented quite well by the neutral density. Therefore, the total sodium density also has a local maximum on the axis and an off-axis minimum, although the radial location of the minimum is somewhat different than indicated in Fig. 5(b).

Sensitivity tests: To determine the sensitivity of the results to the parameters associated with the diagnostic procedure, the following checks were carried out:

(1) For the results presented, the Abel inversion was carried out to the radius at which the intensity was about 1% of its maximum value. To check the sensitivity of the results to this value, temperature profiles were also obtained with cutoff points at 10% and 0.1%. With 10%, the shapes of the temperature profiles did not differ significantly from those with 1%, while with the cutoff point at 0.1% the temperature distributions did change significantly; the signal-to-noise ratio was poor, and the slope of the temperature profile at the cutoff radius (and, therefore, the shape of the parabolic extension) became sensitive to the cutoff value. However, the resulting pressure varied only from 4200 to 4600 Torr when the cutoff intensity was reduced from its maximum to its minimum value.

(2) The starting value of pressure for the iteration was varied over a wide range to verify that the results were independent of that parameter. Poor initial values led simply to increases in number of iterations to reach the same results.

(3) The wall temperature was varied from 800 K to 1200 K. Although the sodium density near the wall varied considerably, the density throughout most of the cross section varied relatively little (by only about 1% at the axis and less than 3% over the radii plotted), and the resulting pressure varied only from about 4100 to 4500 Torr.

(4) The mercury dose was taken to range from 27 to 29 mg, exceeding the actual uncertainty, with no appreciable effect on either the pressure or temperature distributions; the sodium density varied from its nominal values by only about 2.5%, while the core temperature varied by less than 1%.

(5) The axial temperature in the cylindrical end regions was increased from the nominal 1500 to 2400 K, the measured electrode tip temperature. Although the resulting pressure increased by about 6%, the calculated temperatures in the main volume decreased by less than about 0.4% and the sodium densities decreased by no more than about 6%.

(6) Since there is some uncertainty associated with the mercury transition rate, and since values reported in the literature vary by nearly a factor of 2, tests were performed using several values above and below a nominal rate given by Mosburg and Wilke.[22] It was found that halving this nominal value increases the core temperature by about 8% and decreases the Na density by about 15%. Doubling the transition rate yields about a 1% decrease in core temperature and an 8% increase in Na density.

(7) In order to check the ability of the Abel inversion routine to resolve spatial features, we used analytical test cases for the intensity profiles. These profiles were given by a channel model for the emission coefficient; that is, the emission coefficient is uniform at one value within a given radius and uniform at a different value at larger radii. Using a range of step widths and heights encompassing those encountered in the actual data analysis, we found that although quantitative details were not accurately reproduced, the routine properly represented the approximate widths and magnitudes of both local maxima and minima at the axis. Thus, although there is some uncertainty in the values of the temperatures and densities presented in Fig. 5, the distributions should be reliable in their qualitative features. For example, the appearance of axial maxima in sodium number density should not be artifacts of the analysis.

To summarize, we have demonstrated a method for determining two-dimensional temperature and additive density distributions as well as the pressure in an enclosed high-pressure arc. This method can be implemented in various ways. For example, rather than using photographic data-acquisition techniques, one might record the transverse intensity scans by electronic imaging devices coupled to computers to allow rapid implementation of the procedure and for time-resolved measurements. The method presented here is an extension of established diagnostic approaches. It is relatively straightforward to apply and appears capable of disclosing features of the discharge related to important material and energy transport processes.

ACKNOWLEDGMENTS

The authors are grateful to A. H. Bellows for valuable consultation on photographic issues and to J. T. Fairbanks for assistance with computer programming.

APPENDIX: SODIUM EMISSION COEFFICIENT

The spectral region used for sodium is located on the long wavelength wing of the resonance lines. In this region the broadening by neutral mercury atoms can be interpreted in terms of the adiabatic potential for the binary interaction of an excited sodium atom and a ground-state mercury atom.[23] To relate the *D*-line emission to the sodium density, we use an approach[24] developed to describe potential curves for alkali-rare gas excimers. This approach uses the quasistatic theory of line broadening to describe the emission spectrum. For the spectral region of interest the Na*-Hg interaction is described using a Lennard–Jones 8,6 potential with the minimum determined from atomic scattering data.[25] The ground state of the NaHg molecule has a very shallow van der Waals minimum, but is otherwise repulsive. Thus, the emission is bound-free and is characterized by a continuous spectrum, with a correspondence between the frequency of emission and the internuclear separation. The emission coefficient (power radiated per unit volume per unit solid angle per unit frequency interval) at frequency ν and at position (r,z) in the arc is given by

$$\epsilon_{Na}(r,z) = (4\pi)^{-1} n_\nu^*(r,z) h\nu A(\nu), \quad \text{(A1)}$$

where n_ν^* is the number density of excited sodium atoms that are in a molecular state capable of radiating in a frequency interval $\delta\nu$ at frequency ν, and $A(\nu)$ is the molecular transition probability, which is in general a function of frequency, and, therefore, a function of the internuclear separation. For a sodium atom to be included in n_ν^* it must be appropriately perturbed by a neighboring mercury atom. Thus, the density n_ν^* is given by

$$n_\nu^* = 4\pi n^* n_{Hg}(r,z) R^2(\nu) |\delta R(\nu)/\delta\nu| P(\nu), \quad \text{(A2)}$$

where n^* is the total number density of atoms in the appropriate upper state of the atom, n_{Hg} is the ground-state (or essentially the total) number density of mercury atoms, R is the internuclear distance, and $P(\nu)$ is the population factor. The quantity $4\pi R^2 \delta R$ is the volume of the spherical shell between R and $R + \delta R$ within which a mercury atom must be located in order to perturb the excited sodium atom appropriately to radiate in the frequency interval between ν and $\nu + \delta\nu$. The probability of such a binary interaction is proportional to the number of Hg atoms in that shell.

The factor $P(\nu)$ contains the statistical relationship between the excited state population capable of radiating at frequency ν and the excited-state population of isolated excited sodium atoms. That factor is given by

$$P(\nu) = (g_{mu}/g_{fu}) \exp[-\Delta V_u(R)/kT(r,z)], \quad \text{(A3)}$$

where the ratio of the statistical weight factors g_{mu} and g_{fu} accounts for the possibility of there being more than one molecular state that can be formed by an excited Na atom and a ground-state Hg atom—g_{mu} is for the molecular state of interest, g_{fu} is for the free excited atom—and the Boltzmann factor accounts for the difference in potential energy between the perturbed state corresponding to the internuclear separation R and the free state corresponding to infinite separation; $\Delta V_u(R)$ is the difference $V_u(R) - V^*$ between the excited state potential energy $V_u(R)$ at separation R and the excited state potential energy V^* at infinite separation.

The density n^* is given by the Boltzmann relation

$$n^*/n_{Na} = [g_{fu}/U(T)] \exp(-V^*/kT), \quad \text{(A4)}$$

where n_{Na} is the total number density of Na atoms, g_{fu} is the statistical weight of the free Na atom excited state, V^* is the energy of that state, and $U(T)$ is the neutral partition function, which is given by the summation over all states of the quantity $g_i \exp(-V_i/kT)$. Since the partition function is only weakly dependent on temperature,[16] we replace $U(T)$ with a representative value $\bar{U}$. Thus, with the local mercury number density n_{Hg} given by $n_{Hg}(r,z) = p_{Hg}/kT(r,z)$, we substitute Eqs. (A2)–(A4) into Eq. (A1) to obtain

$$\epsilon_{Na}(r,z) = \frac{g_{mu}}{\bar{U}} n_{Na}(r,z) \frac{p_{Hg}}{kT(r,z)} h\nu A(\nu) \times R^2 e^{-[\Delta V_u(R) + V^*]/kT(r,z)} \left|\frac{dR}{d\nu}\right|. \quad \text{(A5)}$$

The potential $\Delta V_u(R) + V^*$ in the exponent represents the potential of NaHg* at the internuclear separation R corresponding to frequency ν.

In using Eq. (A5), we assume the change in the potential is small over the filter bandpass. The quantity $A(\nu)$ varies[26] as the cube of the frequency. However, since our frequency is close to the frequency at line center, we take the transition rate to be that for the resonant atomic transition.[27]

[1] J. F. Waymouth, W. M. Keeffe, W. I. Bamberg, P. J. Gardner, W. Walter, and D. Work, in *Proceedings of the Symposium on Incoherent Light Sources*, Loughborough, U.K., 1975, edited by J. Raffle, (Institute of Physics, Bristol, England, 1975), p. 21.
[2] W. M. Keeffe, IEE Proc. **127**, Pt. A, 181 (1980).
[3] R. J. Zollweg, J. Appl. Phys. **49**, 1077 (1978).
[4] T. Fohl, J. Illum. Eng. Soc. **4**, 265 (1975).
[5] E. Fischer, J. Appl. Phys. **47**, 2954 (1976).
[6] For a review of a number of diagnostic techniques, see W.J. van den Hoek, Philips J. Res. **38**, 188 (1983).
[7] Th. Zaengel and E. Groiss, in *Proceedings of the 3rd International Symposium on the Science and Technology of Light Sources*, Toulouse, France, 1983, edited by D. Blanc (Paul Sabatier University, Toulouse, France, 1983), p. 110.
[8] G. R. Allen, R. Lagushenko, J. Maya, and W. M. Keeffe, in *Proceedings of the Illuminating Engineering Society Conference*, Boston, 1986, edited by A. P. Wasdyke (Illum. Eng. Society of North America, New York, 1986), p. 668.
[9] W. M. Keeffe, Z. K. Krasko, H. L. Rothwell, Jr., and C. W. Struck, Proceedings of the Symposium on Science and Technology of High Temp. Light Sources, Electrochemical Society Meeting, Toronto, 1985, Vol. 85-2, p. 15.
[10] H. P. Stormberg and R. Schafer, J. Appl. Phys. **54**, 4338 (1983).
[11] H. L. Rothwell, Jr. and W. M. Keeffe, J. Illum. Eng. Soc. **10**, 40 (1980).
[12] R. J. Zollweg, J. Illum. Eng. Soc. **8**, 126 (1979).
[13] R. J. Zollweg, J. J. Lowke, and R.W. Liebermann, J. Appl. Phys. **46**, 3828 (1975); J. J. Damelincourt, D. Karabourniotis, L. Scoarnec, and P. Herbet, J. Phys. D **11**, 1029 (1978).
[14] Measurements of optical depth in higher-power metal-halide lamp arcs with similar core temperatures and similar mercury line densities yield transmissions greater than about 90% (H. L. Rothwell, Jr. and W. M. Keeffe, GTE Sylvania Lighting Center, Danvers, MA, Lab. Rpt. No. LR-104, 1979). For sodium a standard double-pass spectroscopic procedure (J. C. Morris, private communication) was carried out over the entire line. For wavelengths greater than approximately 591 nm, the transmission was found to be essentially 100%.
[15] W. L. Barr, J. Opt. Soc. Am. **52**, 885 (1962).
[16] W. Walter of GTE Lighting has evaluated partition functions for a range of arc lamp conditions and has found that the partition functions for mercury and sodium are only weakly dependent on temperature. (GTE Sylvania Lighting Center, Danvers, MA, Lab. Rpt. No. LR-10, 1973.) Thus, we can replace the mercury and sodium partition functions with representative values.
[17] W. M. Keeffe, GTE J. **1**, 39 (1974).
[18] J. F. Waymouth, J. Light Vis. Env. (Illum. Eng. Inst. Japan) **6**, 53 (1982).
[19] P. C. Drop and R. Lorenz, Lichttechnik **28**, 56 (1976).
[20] Small local density maxima on the axis have also been observed by J. T. Dakin and R. P. Gilliard [J. Appl. Phys. **62**, 79 (1987)]. Although in that reported experiment much of the axial convection has been eliminated, the remaining axial nonuniformities and end effects may allow enough axial convection to make our suggested explanation applicable to that case as well.
[21] See, e.g., J. Richter, in *Plasma Diagnostics*, edited by W. Lochte-Holtgreven (North-Holland, Amsterdam, 1968), p.15.
[22] E. R. Mosburg, Jr. and M. D. Wilke, J. Quant. Spectrosc. Radiat. Trans. **19**, 69 (1978).
[23] A. Gallagher, in *Atomic Physics*, edited by G. zu Putlitz, E.W. Weber, and A. Winnacker (Plenum, New York, 1975), Vol. 4, p. 559.
[24] R. E. M. Hedges, D. L. Drummond, and A. Gallagher, Phys. Rev. A **6**, 1519 (1972).
[25] L. Huwel, J. Maier, and H. Pauly, J. Chem. Phys. **76**, 4961 (1982).
[26] G. Herzberg, *Molecular Spectra and Molecular Structure I: Spectra of Diatomic Molecules*, 2nd ed. (Van Nostrand, New York, 1950), p. 20.
[27] Wavelengths and Transition Probabilities for Atoms and Atomic Ions, compiled by J. Reader, C. Corliss, W.L. Wiese, and G.A. Martin, NBS Publ. No. NSRDS-NBS 68, Dec., 1980.